PAGEOPH, Vol. 132, Nos. 1/2 (1990) 0033–4553/90/020331–32$1.50 + 0.20/0

Q Measurements for Phase X Overtones

EMILE A. OKAL[1] and BONG-GON JO[1, 2, 3]

Abstract—Linear stacking procedures are used to retrieve the attenuation of 91 modes belonging to the 3rd, 4th and 5th Rayleigh overtones branches in the 80–160 s period range, and contributing to the so-called "Phase X" wave group. Our data show in general slightly less attenuation than expected from available models. Data space inversion shows that, when combined with previously measured fundamental mode Q's, this new dataset improves resolution significantly in the 1000–2000 km depth range. Based on this remark, we carry out a number of parameter space inversions. Our results suggest a narrow (80–200 km) zone of high attenuation ($Q_\mu = 75-90$), low attenuation in the intermediate mantle (670–1500 km); ($Q_\mu \approx 350$), and lower values in the deeper mantle ($Q_\mu \approx 200$).

Key words: Mantle attenuation, spheroidal overtones.

1. Introduction

Our understanding of anelastic attenuation in the deeper parts of the earth (obtained principally from amplitude measurements on seismograms) has not reached a level of precision comparable to the picture we now have of these regions' elastic properties (obtained mostly from travel-time and dispersion information, and including some insight into their lateral variations). This is not surprising since the dispersion information in a seismogram is usually based on an inherent concept of extremal travel-time, and is therefore a robust observable, remaining to a large extent unaffected by such possible unknowns as precise source characteristics, exact instrument response, scattering, mode conversion (e.g., Love to Rayleigh), receiver crustal structure, and even to a certain extent multipathing, while on the other hand, all these factors affect crucially the amplitude measured on the resulting seismogram.

[1] Department of Geological Sciences, Northwestern University, Evanston, Illinois 60201, U.S.A.
[2] Also: Department of Geology and Geophysics, Yale University, New Haven, Connecticut 06511, U.S.A.
[3] Now at: Department of Geology, Jeonbug National University, Jeonju, Jeonbug 520, Republic of Korea.

Most available Q models have little if any resolution in the deeper mantle. The early multi-layered models of ANDERSON and HART (1978) were clearly over-parameterized, at the cost of instability; NAKANISHI (1981) solved for about 12 layers of Q_μ in the mantle, but indicated that his dataset lacked resolution in the deeper mantle. Using data space inversion, STEIN *et al.* (1981) concluded that their dataset has practically no resolution below 1500 km. More recent models, such as MASTERS and GILBERT's (1983) provided some insight into the attenuation of the lowermost mantle and inner core, but had little resolution in the intermediate mantle. Finally, in presenting their Preliminary Reference Earth Model [PREM], DZIEWONSKI and ANDERSON (1981) emphasized that theirs was a rough model, whose stated primary goal was only to provide a satisfactory way of accounting for the influence of dissipation on dispersion (KANAMORI and ANDERSON, 1977).

Among the various models discussed by SAILOR and DZIEWONSKI (1978), we retain Model "QKB," which features only two layers in the mantle, but has a finite Q_K in the upper mantle (low-velocity zone) and inner core. These authors determined that the resolution of their data was insufficient to warrant any finer layering of the planet.

One of the reasons for the lack of resolution of the above studies in the intermediate mantle, is that most of them strongly emphasized fundamental normal modes, due in large part to their preponderance in the seismic signal. Because the resolving kernels of the fundamentals are basically similar to each other, increasing the dataset results in only marginal improvement of the resolution. On the other hand, surface wave overtones are characterized by eigenfunctions, and therefore resolving kernels, whose shapes differ significantly from those of their fundamental counterparts of comparable periods. The measurement of their attenuation is expected to substantially improve our resolving power for intrinsic attenuation in the mantle.

Specific studies of overtone attenuation have included DRATLER *et al.* (1971), SMITH (1972) and NOWROOZI (1974), who measured some overtone Q values applying the time rate decay method. ROULT (1974, 1975) and JOBERT and ROULT (1976) applied a time variable filtering technique to isolate individual overtone branches before measuring their attenuation; this method, however, cannot be applied when overtone branches intersect in the frequency-group velocity plane.

Prominent among mantle overtones in the 80–150 s period range are the so-called "Phase X" modes, observed principally on the radial "away-from-the-source" components of seismograms. They were first recognized (and the name Phase X coined) by JOBERT *et al.* (1977), and identified by JOBERT (1978) as due to a superposition of the third, fourth and fifth higher Rayleigh modes ${}_3R$, ${}_4R$, and ${}_5R$, travelling at the same group velocity ($\simeq 6$ km/s) in this frequency range. In a series of previous studies (OKAL and JO, 1985, 1987 (hereafter Papers 1 and 2)), we discussed stacking methods allowing separation of the branches, and presented extensive dispersion datasets for the three branches. More recently, TANIMOTO

(1987) has inverted substantial Phase X datasets to obtain refined models of shear wave lateral heterogeneity inside the earth. In the present study, we obtain Q measurements for approximately 100 modes belonging to the Phase X branches, and conduct a preliminary inversion of the dataset, augmented by a set of fundamental modes. We refer to Papers 1 and 2 for a description of the general properties of Phase X. In particular, we use the notation ${}_p\Sigma_l$ to denote a mode of angular order l belonging to the physically continuous p-th overtone branch; because of the presence of a branch of Stoneley modes, the conventional nomenclature for such a mode could be ${}_nS_l$ with either $n = p$ or $n = p + 1$ (OKAL, 1978). We occasionally keep the notation ${}_pS_l$ when $n = p$.

2. Q Measurements

2.1. Methodology

• *The Choice of a Method.* Our purpose is to retrieve the temporal attenuation Q of the modes composing Phase X. Among the many methods which have been used to retrieve the attenuation of surface waves or normal modes, we retain the measurement of the width of a spectral peak first used by NESS *et al.* (1961). It consists of modeling the spectral amplitude of an attenuated normal mode of angular frequency ω_0 as:

$$|A(\omega)| = A_0 \cdot \left| \frac{1}{\alpha - i(\omega_0 - \omega)} + \frac{1}{\alpha + i(\omega + \omega)} \right| \tag{1}$$

where $Q = \omega_0/2\alpha$. In practice, and given a Fourier spectrum in the vicinity of ω_0, the best-fitting parameters A_0, ω_0, and α are easily obtained by using a trial and error algorithm due to SAILOR and DZIEWONSKI (1978), which minimizes the root-mean-squares misfit

$$\left(\sum_i \left[\ln\left(\frac{A_{\text{observed}}}{A_{\text{computed}}} \right)_i \right]^2 \right)^{1/2}, \tag{2}$$

summed over frequencies ω_i, and where A_{computed} is given by (1).

We also considered other methods, including the time-domain amplitude decay of a narrow-bandpass filtered record (ALSOP *et al.*, 1961; STEIN and NUNN, 1981); the analytical continuation of seismic spectra (BULAND and GILBERT, 1978); the complex demodulation method (HANSEN and BOLT, 1980); and the use of spectral line amplitudes as a relative measurement of Q factors (MASTERS and GILBERT, 1981; 1983). In a previous study (OKAL, 1980; OKAL and STEIN, 1981), we tested the equivalence and performance of these various methods, and concluded that their results were consistent within 5%. Thus, we selected the first method (fitting a lineshape in the frequency domain); most other methods involve extensive computation, since they require Fourier transforming every time a bandpass filter is applied

(time-domain measurements), or for each value of the trial parameters (analytical continuation or complex demodulation).

• *Stacking*. Because of the crossover in group velocity between the various branches making up Phase X, it is impossible to isolate records belonging to a single branch at a given station. In addition, and as we will see *a posteriori*, the Q values of the various branches are themselves close to each other, so that several branches with directly comparable *complex* eigenfrequencies arrive at similar group times in the seismograms. In this respect, a technique such as FUKAO and SUDA's (1987), which allows separation of modes with similar frequencies but different Q values, would not work in the case of Phase X.

Consequently, some form of stacking is mandatory for the retrieval of the attenuation properties of Phase X branches. We follow the general approach of Paper 2, but of course restrict ourselves to linear stacking in order to preserve the amplitude information in the seismograms.

Specifically, and when targeting a particular mode ${}_p\Sigma_l$ ($p = 3, 4$ or 5), we compute its excitation along the horizontal, away from the source, component

$$E_j = \left[K_0 s_R \frac{dP_l^0}{d\theta} - K_1 q_R \frac{dP_l^1}{d\theta} + K_2 p_R \frac{dP_l^2}{d\theta} \right] \tag{3}$$

at each station j, and form the scalar product $\Sigma_{j=1}^{J} E_j^* a_j(\omega)$ (where a_j is the spectral amplitude at the j-th station, and J the total number of stations), in the vicinity of $\omega = {}_p\omega_l$; the notations are those of KANAMORI and CIPAR (1974). This stacking technique was introduced by MENDIGUREN (1973) and DZIEWONSKI and GILBERT (1973).

• *Correction for Systematic Bias*. As in the case of dispersion, ellipticity and lateral heterogeneity (and, to an extent negligible in the frequency range considered, earth rotation), combine to affect measurements of the attenuation of mantle overtones taken from stacked spectra. In general, the presence of the various singlets, and destructive interference between them, leads to artificially low values of Q. The quantification of this systematic bias has been studied by DAHLEN (1979) from a theoretical standpoint, and SLEEP *et al.* (1981) from a statistical one. If w is the total width of the multiplet in the angular frequency domain, Dahlen has shown that the apparent value α_{app} of true decay constant $\alpha_0 = \omega_0/2Q_0$ must satisfy:

$$\alpha_0 \leq \alpha_{app} \leq \alpha_0[1 + w^2/4\alpha_0^2], \tag{4}$$

so that the bias in Q can be bracketed as

$$Q_{app} \leq Q_0 \leq Q_{app}\left[1 + \frac{w^2 Q^2}{\omega_0^2}\right] \tag{5}$$

where the terms neglected are fourth order in (wQ/ω_0).

In order to assess the possible bias in our measurements, we need to estimate the width w of the multiplet, due to earth rotation, ellipticity and structural lateral

heterogeneity. The computation of rotation and ellipticity parameters for the Phase X modes, as well as results regarding heterogeneity on fundamental modes (SILVER and JORDAN, 1981; SLEEP *et al.*, 1981), and our own results on overtones from Paper 2 and JO (1986), all suggest that an upper bound to the width for the modes making up Phase X is:

$$w/\omega_0 = 2 \times 10^{-3}. \tag{6}$$

We will see that typical values of overtone Q's are on the order of 250. As a result, the maximum bias predicted for this method is an *overestimation* of the attenuation (or *underestimation* of Q) by about 25%. As a consequence, we correct the results by adding an *average* bias of 12% to measured Q values. In addition, we assign a systematic uncertainty of $\pm 12\%$ to all measurements.

• *Estimation of Precision.* Direct estimation of further uncertainties inherent in a stacking method is practically impossible. MENDIGUREN (1973) proposed to use subsets of stations, and to estimate the uncertainty in the results from a measure of the possible scatter of results when using different subsets. This technique, which works well when the number of stations is large (he was using up to 84), clearly cannot be applied to our case, where we deal with at most 12 stations. A measure of the scatter resulting from a possibly different sampling of the earth by rays emanating from different earthquakes can be used to estimate further the precision of the method. For each mode, our dataset is limited to a typical average of 3 events. The scatter in their results is on the order of a few percent. Our final standard deviation is the value of 12% described above, plus any scatter between results from different events.

In applying the amplitude matching techniques to the data, we made iterations for 30 trial values of α and of the resonant frequency ω_0, centered around their theoretical values for PREM.

2.2 Test Runs

In order to assess the validity of the method, and especially of the corrections used to counter the systematic bias due to ellipticity and heterogeneity, we performed a series of test runs of this method on synthetic data involving fundamental modes. Table 1 and Figure 1 summarize this experiment.

Specifically, we synthetize the spectra of 10 seismograms in the 150–500 s period range for a geometry representative of our Phase X experiments. Our first synthetics use the spherically symmetric PREM model. We use a realistic geometry, involving the epicenter of Event 2 (see Table 2) and 10 GDSN stations: ANMO, COL, CHTO, GRFO, MAIO, MAJO, NWAO, SJG, SUR, ZOBO. This geometry and the number of stations were chosen to randomize as much as possible the distances and azimuths to the stations, while keeping the test representative of our Phase X dataset. In this experiment, we target three modes (${}_0S_{13}$, $T = 473.31$ s; ${}_0S_{29}$, $T = 268.41$ s; and ${}_0S_{59}$, $T = 155.24$ s), covering the ranges of both frequency and

TEST RUNS ON STACKED SYNTHETICS

SPHERICAL EARTH

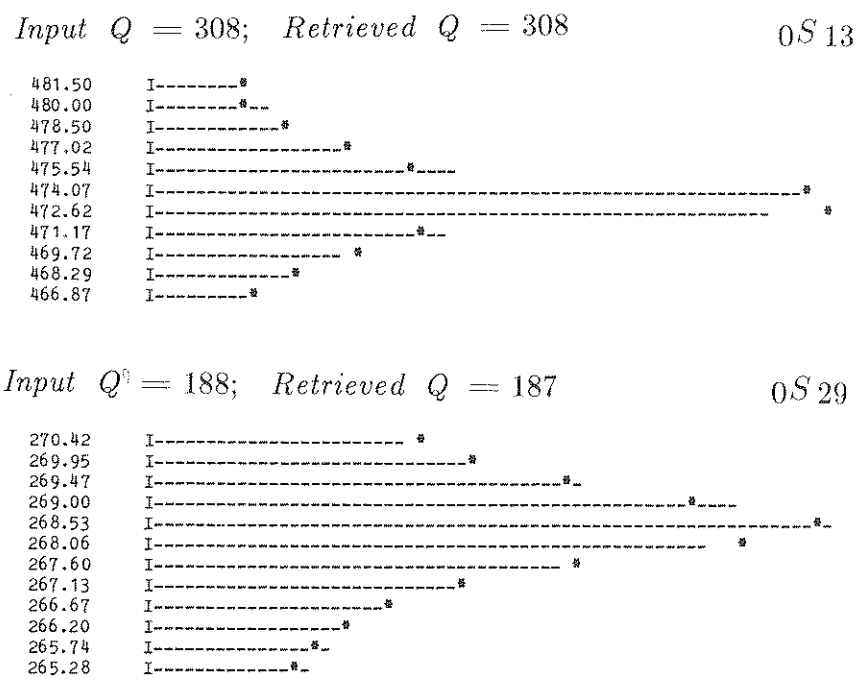

Figure 1a

Examples of the determination of mode Q's by fitting a resonance curve (dashes) to the stacked spectral line (stars). Numbers at left are periods for discretized FFT frequencies. In this case, we are testing a stack of ten synthetic spectra, computed for a spherical earth (see text and Table 1 for details).

TEST RUNS ON STACKED SYNTHETICS

HETEROGENEOUS [M-84] ELLIPTICAL EARTH

Input $Q = 308$; *Retrieved* $Q = 274$ $0S\,13$

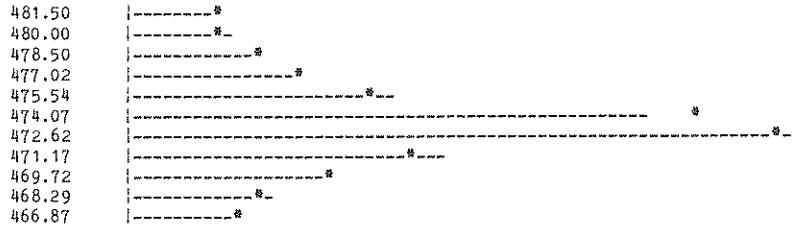

Input $Q = 188$; *Retrieved* $Q = 172$ $0S\,29$

Input $Q = 136$; *Retrieved* $Q = 114$ $0S\,59$

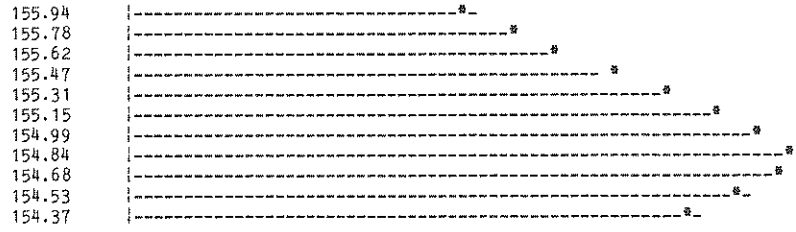

Figure 1b

Same as Figure 1a for a stack of ten synthetic spectra, computed with the effect of ellipticity and heterogeneity; note systematic low bias in the values of Q retrieved by this procedure.

Table 1

Results of stacking tests on fundamental modes

Mode	${}_0S_{13}$	${}_0S_{29}$	${}_0S_{59}$
Original Values Used in Synthetics			
Period (s)	473.31	268.41	155.24
Q_0	308	188	136
Stacked Values (Radially Symmetric Model)			
Q_{app}	308	187	129
Stacked Values (Model M84 with Ellipticity)			
Q_{app}	274	172	114
Deviation $\frac{Q_{app}}{Q_0} - 1$	12.4%	9.3%	19.3%
$\frac{w^2Q^2}{\omega_0^2}$	26%	20%	23%

wavelength of the Phase X experiments. We then stack the records according to equation (3), and obtain the estimate (Q_{app}) by best-fitting equation (1) to the spectrum. The conclusion of this experiment is that for a spherically symmetric earth, stacking is a legitimate method for retrieving Q.

We then proceed to build new synthetics, including ellipticity and lateral heterogeneity corrections according to WOODHOUSE and DZIEWONSKI's (1984) Model M84, and following the formalism outlined by these authors and DAHLEN (1975). We then proceed to stacking and fitting the resonance curve, as if the earth were spherically symmetric. Table 1 clearly shows that the resulting values of Q_{app} are systemically too low, by an amount ranging from 10 to 20%.

We then compare this bias to the predictions of DAHLEN (1979) by computing the width w of the mode, which we define as the maximum interval $\omega_i - \omega_j$ of the apparent angular frequencies at two stations i and j in our "synthetic" set. In all cases, we verify that DAHLEN (1979) gives an accurate estimate of the systematic bias introduced by ellipticity and lateral heterogeneity; a correction of the type proposed in Section 2.1 above would in all cases result in an acceptable bracket for the true value Q_0. In conclusion, these test runs justify the corrections described in Section 2.1.

The effect of the winnowing and tapering necessary to suppress the fundamental and extract the overtones (see Paper 2) was also investigated. It can displace the value of Q, by a maximum amount of 2%, negligible in view of the larger uncertainties described above.

Table 2

Epicentral and focal parameters of earthquakes used in this study

Event Number	Region	Date YMD	Origin Time GMT	Epicenter °N	Epicenter °E	Depth (km)	Moment (10^{27}dyn-cm)	Focal Mechanism ϕ(°)	δ(°)	λ(°)	Reference
1	Colombia	1979 12 12	07:59:04.4	1.62	−79.34	28	20	179	78	83	a
2	Santa Cruz	1980 07 17	19:42:23.2	−12.52	165.92	33	8	142	63	70	b
3	Banda Sea	1982 06 22	04:18:40.5	−7.34	126.04	450	2	310	70	225	c
4	New Ireland	1983 03 18	09:50:50.0	−4.88	153.58	85	6.7	49	54	79	a
5	Costa Rica	1983 04 03	02:50:01.1	8.72	−83.12	33	0.5	305	15	90	d

(*)Focal mechanism notations are those of KANAMORI and CIPAR (1974). References to focal mechanisms are: (a): ROMANOWICZ and GUILLEMANT (1984); (b): KANAMORI and GIVEN (1982); (c): DZIEWONSKI *et al.* (1983a); (d): DZIEWONSKI *et al.* (1983b).

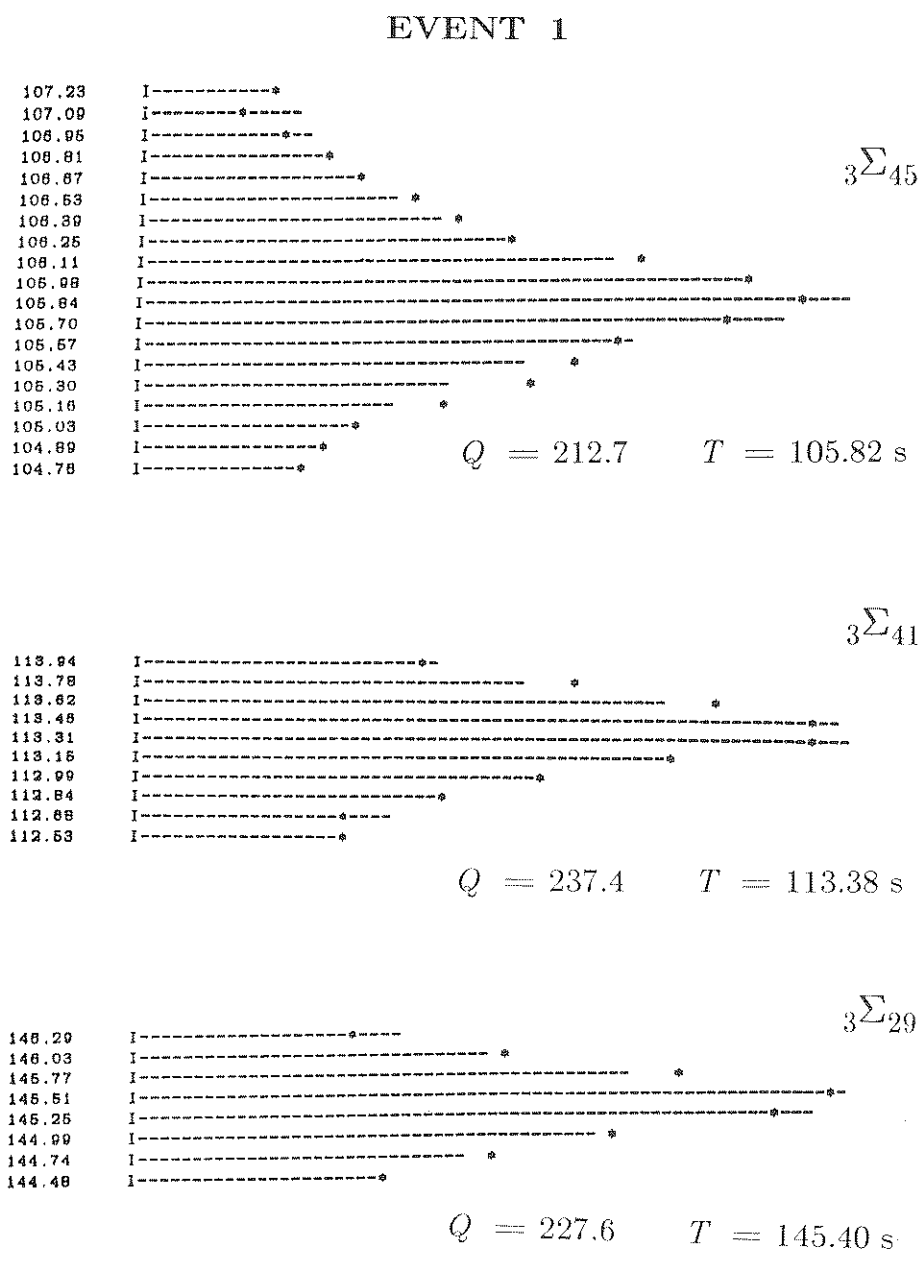

Figure 2
Examples of the determination of mode Q's by fitting a resonance curve (dashes) to the stacked spectral line (stars). The resulting values of the center period, and Q are given for each diagram.

Table 3a

Q data for spheroidal normal modes of the third overtone branch ${}_3\Sigma_l$ contributing to the X phase

Angular Order l	ATTENUATION FACTOR Q									
	Measured (Events)					Mean				Computed
	1	2	3	4	5	Q	Q_c corrected	Q_c^{-1} ($\times 100$)	σ ($\times 100$)	PREM
25		269.8				269.8	302.2	0.3309	0.0397	258.9
26		263.4				263.4	295.0	0.3390	0.0407	258.4
27	263.2	278.0				270.4	302.8	0.3302	0.0539	257.8
28	277.2	259.5				268.1	300.2	0.3331	0.0574	257.1
29	260.4	237.7		232.7		243.0	272.2	0.3674	0.0683	255.9
30	254.9			230.9	284.0	254.8	285.3	0.3504	0.0825	254.5
31		229.5		234.8		232.1	260.0	0.3847	0.0531	252.9
32		235.9	258.9		255.8	249.8	279.7	0.3575	0.0634	251.1
33	243.7	211.6	248.1			233.3	261.3	0.3827	0.0841	249.0
35		247.6	242.6		243.9	244.7	274.0	0.3649	0.0481	244.3
36	248.7	235.5	211.2		231.6	230.9	258.7	0.3866	0.0762	241.7
37	216.0	232.2			252.0	232.5	260.4	0.3841	0.0792	239.1
38	226.2	245.4	248.6		245.5	241.1	270.0	0.3704	0.0628	236.3
39					245.1	245.1	274.5	0.3643	0.0437	233.4
40	230.2				234.0	232.1	259.9	0.3847	0.0512	230.6
41	218.1		222.8	190.7	226.3	213.5	239.1	0.4182	0.0881	227.7
42	222.0	214.4		191.2	221.3	211.4	236.8	0.4223	0.0848	225.0
43	210.6	209.4			212.6	210.9	236.2	0.4234	0.0544	222.2
44	207.9	207.5		195.9	214.1	206.1	230.9	0.4331	0.0702	219.6
45	212.7			199.7		206.0	230.7	0.4334	0.0737	217.0
46					202.6	202.6	226.9	0.4407	0.0529	214.6
47		193.8	211.4			202.2	226.5	0.4415	0.0834	212.1
48			221.7			221.7	248.3	0.4027	0.0483	209.6
49	227.4				198.4	211.9	237.3	0.4213	0.0960	206.9
50	214.7				200.3	207.3	232.1	0.4308	0.0754	205.2
51	199.8	197.5	219.3			205.1	229.7	0.4354	0.0798	203.5
52					201.4	201.4	225.6	0.4433	0.0532	201.9
53		188.7				188.7	211.3	0.4732	0.0568	200.3
54		199.3				199.3	223.2	0.4480	0.0538	198.2
55		176.3				176.3	197.5	0.5064	0.0608	196.9
56				196.1	203.3	199.6	223.6	0.4472	0.0664	195.7
57	190.8					190.8	213.7	0.4680	0.0562	194.5
58	179.8		186.2			182.9	204.9	0.4880	0.0721	193.4
59	184.1	192.2		174.0		183.1	205.1	0.4876	0.0858	192.4
60	182.8					182.8	204.7	0.4884	0.0586	191.4
61		183.9				183.9	206.0	0.4855	0.0583	190.6
62	160.6					160.6	179.9	0.5560	0.0667	189.3

2.3 Dataset

The dataset in this study is a subset of the GDSN long-period records used for the dispersion investigation in Paper 2. Table 2 lists epicentral and focal mechanism parameters of earthquakes used in the present study. Since we do not have access to the enhanced resolution of the nonlinear stacking, the number of usable data for the present study is smaller than that of eigenperiods identified in Paper 2.

In practice, we use a number of stations J varying from 8 to 12, with records of 20 hr duration. We eliminate most of the fundamental mode signal by winnowing

Table 3b
Q data for spheroidal normal modes of the fourth overtone branch ${}_4\Sigma_l$ contributing to the X phase

Angular Order l	ATTENUATION FACTOR Q									
	Measured (Events)					Mean				Computed
	1	2	3	4	5	Q	Q_c corrected	Q_c^{-1} ($\times 100$)	σ ($\times 100$)	PREM
20	252.3	304.3				275.9	309.0	0.3237	0.0867	279.1
21		306.1				306.1	342.8	0.2917	0.0350	275.1
24		267.1				267.1	299.2	0.3343	0.0401	265.9
25	267.4	254.1				260.6	291.9	0.3426	0.0550	263.0
27					275.3	275.3	308.3	0.3243	0.0389	257.0
28		232.5				232.5	260.4	0.3840	0.0461	254.0
29	270.2		237.9			253.0	283.4	0.3529	0.0779	251.0
30	257.4	254.8			233.0	247.9	277.7	0.3602	0.0657	248.1
31	250.1	248.4				249.2	279.2	0.3582	0.0449	245.3
32	239.2	243.1			240.2	240.8	269.7	0.3708	0.0480	243.0
33	239.1	238.3	225.6		239.0	235.4	263.6	0.3794	0.0578	240.5
35	237.8		230.6	210.4		225.7	252.7	0.3957	0.0761	236.9
36			221.3		231.1	226.1	253.2	0.3949	0.0609	235.5
38	229.0	222.0			223.4	224.8	251.7	0.3972	0.0549	234.2
39	216.9	230.8			234.4	227.1	254.4	0.3931	0.0654	234.3
40	227.5	227.6			229.6	228.2	255.6	0.3912	0.0492	234.1
41	226.3	220.2			235.5	227.2	254.4	0.3931	0.0620	233.9
42	223.5	212.9				218.1	244.2	0.4094	0.0649	233.5
43	239.8		220.8	179.6	220.6	212.8	238.3	0.4196	0.1107	234.7
44	215.3		228.7		235.7	226.2	253.4	0.3946	0.0679	234.3
47	212.5	208.5				210.5	235.7	0.4242	0.0573	236.4
48	224.4	204.9				214.2	239.9	0.4168	0.0800	237.6
49	229.7		234.4			232.0	259.9	0.3848	0.0523	236.5
51			222.8		228.3	225.5	252.6	0.3959	0.0552	238.6
52			203.4	192.8		198.0	221.7	0.4510	0.0732	236.6
53			210.2	203.6		206.8	231.7	0.4317	0.0627	237.4
54		228.5	218.7			223.5	250.3	0.3995	0.0618	238.0
55		212.8				212.8	238.3	0.4196	0.0503	234.7
56	205.0					205.0	229.6	0.4355	0.0523	235.1
57		221.0				221.0	247.5	0.4040	0.0485	234.1

the times series, and keeping only sections corresponding to group arrival velocities between 5.6 and 6.9 km/s for each subsequent passage; while the q-th passage of the fundamental Rayleigh wave ($_0R_q$) may occasionally remain in the winnowed seismogram for one station, its absence both for subsequent passages $_0R_s$, and at other stations, effectively kills the corresponding normal modes from the stacked spectrum.

In Figure 2 we give some examples of the determination of Q values by matching stacked spectral amplitude curves (stars) and computed resonance curves (bars).

2.4 Results

Globally, we obtained 201 measurements of mode Q's, concerning 91 modes belonging to the 3 branches contributing to Phase X: $_3R$, $_4R$, and $_5R$. The resulting Q values are listed in Table 3, and plotted on Figure 3 together with predicted

Table 3c
Q data for spheroidal normal modes of the fifth overtone branch $_5\Sigma_l$ contributing to the X phase

	ATTENUATION FACTOR Q									
	Measured					Mean				Computed
Angular Order l	(Events) 1	2	3	4	5	Q	Q_c corrected	Q_c^{-1} ($\times 100$)	σ ($\times 100$)	PREM
23		280.3	287.8			284.0	318.1	0.3144	0.0443	294.4
24	270.2	263.9				267.0	299.1	0.3344	0.0464	284.8
25	259.8				266.8	263.3	294.8	0.3392	0.0478	276.1
27	265.6	272.0		266.7		268.1	300.2	0.3331	0.0447	263.4
28		259.1	262.4			260.7	292.0	0.3424	0.0445	259.2
31		245.7	257.7		270.1	257.4	288.3	0.3468	0.0600	252.1
32	249.8	249.7	260.6		220.0	244.0	273.3	0.3659	0.0748	250.5
36		236.9	249.3			242.9	272.1	0.3675	0.0589	249.2
37	235.3	243.9				239.5	268.3	0.3728	0.0553	248.4
38	223.7	228.5				226.1	253.2	0.3949	0.0540	247.5
39	224.6	232.6	251.9		204.3	227.1	254.3	0.3932	0.0856	246.0
40	234.2					234.2	262.3	0.3812	0.0457	246.5
41	214.4		225.0			219.6	245.9	0.4066	0.0643	244.4
42		225.9				225.9	253.0	0.3952	0.0474	244.7
43		219.9	210.1			214.9	240.7	0.4155	0.0649	242.0
44		220.4	233.1		200.0	217.0	243.0	0.4115	0.0854	242.1
45		206.6	234.5		229.9	223.0	249.7	0.4004	0.0791	238.6
46		215.5	247.7		228.6	229.9	257.4	0.3885	0.0768	238.5
47		220.1	208.7		237.7	221.5	248.1	0.4030	0.0777	234.5
48		229.9				229.9	257.5	0.3884	0.0466	234.4
49	210.4	213.7	239.8	201.7		215.5	241.4	0.4143	0.0832	234.4
50		215.5	234.6	224.0	220.6	223.5	250.3	0.3996	0.0639	230.3
51				196.3		196.3	219.9	0.4548	0.0546	230.4
52		209.7				209.7	234.9	0.4258	0.0511	230.5

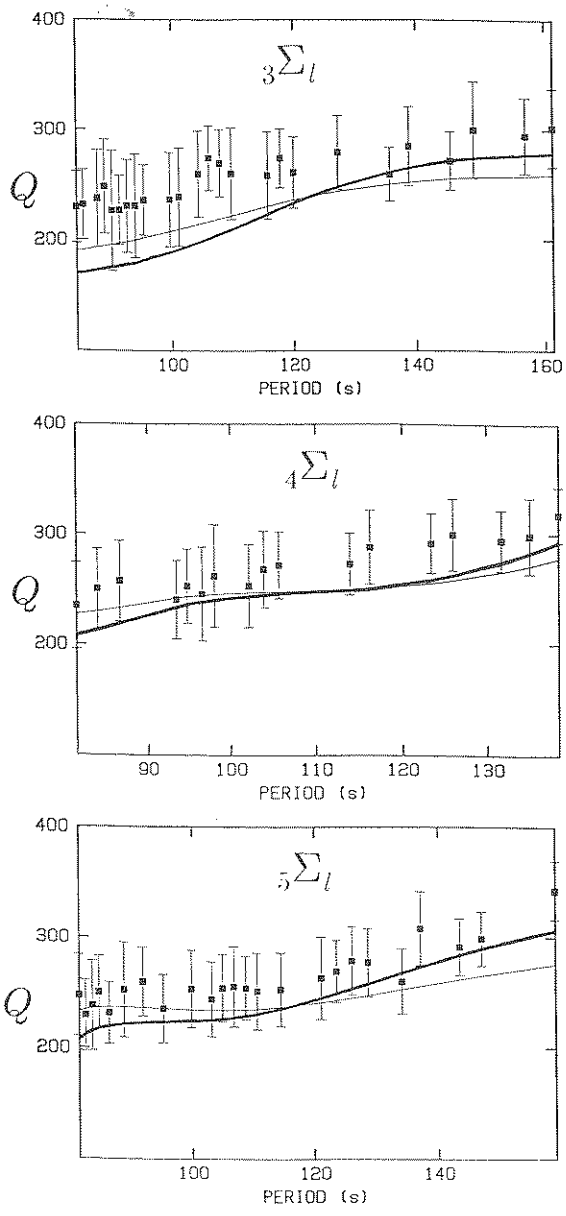

Figure 3
Individual measurements (with error bars) of the attenuation of normal modes from the ${}_3R$, ${}_4R$ and ${}_5R$ branches, as compared to values predicted from models PREM (light trace) and QKB (thick trace).

values obtained from two published models: PREM (DZIEWONSKI and ANDERSON, 1981) and QKB (SAILOR and DZIEWONSKI, 1978). In general, and considering the error bars, our values fall within the range of those two models. ${}_3R$ and ${}_5R$ tend to fit QKB better at lower angular numbers, and PREM better at higher frequency; ${}_4R$ is in general better fit by PREM than by QKB.

3. Inversion

Our goal in the present study is to use our measured overtone Q's in an attempt to increase the resolution of the dataset. We use an enlarged dataset consisting of the above values of overtone Q's, and of a sampling of 38 fundamental spheroidal Q values used by STEIN *et al.* (1981), and originally obtained by SAILOR and DZIEWONSKI (1978), STEIN and GELLER (1978), MILLS and HALES (1977, 1978), GELLER and STEIN (1979), and STEIN and NUNN (1981).

3.1 Methods

We refer to SAILOR and DZIEWONSKI (1978) for a clear and concise description of the problems arising in attempting an inversion for the structural Q_μ and Q_K, due to our generally poor knowledge of even their gross variation inside the earth, and for a review of the general formalisms of data space and parameter space inversions. We will follow these authors' approach in using, in a first step, data space inversion to define the resolution of our dataset, and then utilize the latter results to optimize our parameterization in order to proceed with parameter space inversions.

The two inversion procedures have been described in detail by BACKUS and GILBERT (1967), WIGGINS (1972), and AKI and RICHARDS (1980). Fundamentally, parameter space inversion works well for an overdetermined problem, whereas data space inversion will address the problem of an underdetermined problem. For a given dataset, parameter space inversion will work well if the parameterization is coarse enough, and accurate (e.g., in the case of a layered model of the earth, if the layer discontinuities are distributed properly); data space inversion will avoid the problem of artificial parameter discontinuities due to layering, but will lack the capacity of targeting the influence of specific parameters, such as a finite Q_K^{-1} in the low-velocity zone.

Our specific computer codes were derived from WIGGINS (1976) in the case of parameter space inversion, and from STEIN *et al.* (1981) for data space inversion. The latter uses various techniques due to BACKUS and GILBERT (1968), and GILBERT (1971).

- *Data Space Inversion.* In using this procedure, we follow GILBERT's (1971) method of "ranking and winnowing" the dataset, which basically consists of expanding the data onto a set of information vectors orthogonal to each other, and

featuring decreasing importance and resolution power. Specifically, the problem is to find a distribution of structural Q_μ (hereafter abbreviated as Q) throughout the earth, fitting, in some optimal sense, the various mode Q's:

$$Q_j^{-1} = \int_0^a G_j(r) Q^{-1}(r)\, dr, \tag{7}$$

where the index j refers to a particular mode, and the kernels G_j are readily obtained from the familiar mode partials. The Q^{-1} distribution is sought through its deviation from some starting model

$$\delta Q^{-1}(r) = \sum_i v_i \Gamma_i(r), \tag{8}$$

where the Γ's are the so-called transformed kernels

$$\Gamma_i(r) = \sum_j T_{ij} G_j(r), \tag{9}$$

obtained from the G's by diagonalizing the matrix A_{ij} of the cross-products $\int G_i G_j\, dr$, after weighting it by the respective standard deviations, and ranked in decreasing order of the amplitude of the eigenvalues of A. Under the condition that the resulting model depart as little as possible from the starting model,

$$\int_0^a [\delta Q^{-1}(r)]^2\, dr \text{ minimum} \quad \text{or} \quad \sum_i v_i^2 \text{ minimum}, \tag{10}$$

the coefficients v_i in (8) are simply found as the minimum values of the transformed attenuation data, taking into account the uncertainties σ_j:

$$v_i = \min\left(\left| \sum_j T_{ij} [\delta Q_j^{-1} + \epsilon_{ij} \sigma_j] \right|;\ \left| \sum_j T_{ij} [\delta Q_j^{-1} - \epsilon_{ij} \sigma_j] \right| \right), \tag{11}$$

where ϵ_{ij} is the sign of the product $T_{ij} \delta Q_j^{-1}$ (no sum).

• *Parameter Space Inversion.* The parameter space inversion used here is a variation of the well-known least-squares procedure, taking into account the variance of the data, and some estimate of the maximum variance acceptable in the parameter space, as discussed by WIGGINS (1972).

Specifically, given a dataset of misfits $\delta Q_j^{-1} \pm \sigma_j$ for each mode j, making up a data vector $\delta \mathbf{d}$, and a predetermined number of layers m, we seek corrections to the structural Q's in each layer, δQ_i^{-1}, making up a parameter space vector $\delta \mathbf{p}$. We weight the data according to their variance, and the parameters according to the thickness of the various layers, thus replacing the model matrix $\mathbf{M}$ by a transformed matrix

$$\mathbf{A} = \mathbf{S}^{1/2} \mathbf{M} \mathbf{W}^{1/2} \tag{12}$$

where $\mathbf{S}$ is the variance matrix of the data, and $\mathbf{W}$ is a diagonal $m \times m$ matrix made

up of the inverse thicknesses of the individual layers. We then use singular value decomposition (LANCZOS, 1961) to write the matrix A as

$$\mathbf{A} = \mathbf{U}\Lambda\mathbf{V}^{\mathrm{T}} \tag{13}$$

where Λ is a square matrix, whose dimension is the rank k of the matrix A. In real life, and given noisy data, the rank of a matrix can only be estimated by the *ad hoc* procedure of examining the influence of variations in k on the stability of the problem. Typically, we have been solving for about 7 layers in the solid earth, and have considered 3 or 4 eigenvalues, *i.e.*, $k = 3$ or 4.

The solution is then obtained as:

$$\delta\mathbf{p} = \mathbf{W}^{1/2}\mathbf{V}\Lambda^{-1}\mathbf{U}^{\mathrm{T}}\mathbf{S}^{1/2}\delta\mathbf{d} \tag{14}$$

or $\delta\mathbf{p} = \mathbf{W}^{1/2}\mathbf{V}\delta\mathbf{p}^*$, where the $\delta\mathbf{p}^*$ are the independent transformed parameters. Their variance is obtained by:

$$\mathbf{X}^* = \Lambda^{-1}\mathbf{U}\mathbf{S}\mathbf{U}^{\mathrm{T}}\Lambda^{-1} \tag{15}$$

where S is the variance matrix of the data.

3.2 Starting Models

Both the data space and parameter space inversion methods require a starting model, which allows our data to be expressed as deviations, or misfits. In addition to the available models PREM (DZIEWONSKI and ANDERSON, 1981) and QKB (SAILOR and DZIEWONSKI, 1978), we also use a model of constant Q [QCST] throughout the solid earth (crust, mantle and inner core), with no bulk attenuation Q_κ^{-1} anywhere in the earth. The purpose of QCST as a starting model is primarily to study the depth resolution of our dataset by data space inversion, without introducing any *a priori* bias on the location of possible discontinuities. The homogeneous value of Q_μ in the crust and mantle is taken as 200, a value representative of the order of magnitude of the Q of the body waves ScS_n (NAKANISHI, 1979; SIPKIN and JORDAN, 1980). Model QCST is also included in Table 4. Parameter space inversions are carried out with either of the three starting models.

3.3 Results

• *Data Space Inversion.* Our first inversion experiments consisted of data space inversion runs using QCST as a starting model. The data set consisted of both fundamental modes and overtones. Figure 4 compares the transformed kernels of the first (largest) eigenvalue for a dataset consisting exclusively of the 38 fundamentals, and for the full dataset. It is clear that the overtones give enhanced resolution in the lower mantle, between depths of 1000 and 2000 km, where the transformed

Table 4

Starting Q models used in the inversions

Layer				
	Depth Range			
Nature	(km)	(km)	Q_μ	Q_κ
PREM (DZIEWONSKI and ANDERSON, 1981)				
Ocean	0	3	∞	57822
Crust and Lid	3	80	600	57822
LVZ	80	220	80	57822
Transition zone	220	670	143	57822
Lower Mantle	670	2891	312	57822
Outer Core	2891	5149.5	∞	57822
Inner Core	5149.5	6371	85	1328
QKB (SAILOR and DZIEWONSKI, 1978)				
Crust and Lid	0	80	115	∞
Upper Mantle	80	670	115	742
Lower Mantle	670	2885	395	∞
Outer Core	2885	5154	∞	∞
Inner Core	5154	6371	∞	1227
QCST (Constant Q_μ in solid earth)				
Ocean	0	3	∞	∞
Crust and Mantle	3	2891	200	∞
Outer Core	2891	5149.5	∞	∞
Inner Core	5149.5	6371	200	∞

kernels for fundamentals only remain basically zero. The subsequent eigenvalues of the full problem do not provide significant improvement in the resolution.

The general solution achieved by the data space inversion for the full dataset features lower attenuation than observed for the fundamentals, a generally excellent fit of the branch ${}_5\Sigma_l$, a very good fit of ${}_4\Sigma_l$ except at the longest periods, and an acceptable fit of ${}_3\Sigma_l$ below 120 s (see Figure 5). At these longer periods, the third and fourth branch have measured attenuation values smaller than predicted by the resulting model.

When comparing the Q model resulting from data inversion for the fundamentals on one hand (this is the final model of STEIN *et al.* (1981) and the whole dataset on the other, one notes fundamentally a considerable reduction of the low-Q zone in the upper mantle to the classical "seismic asthenosphere" (say 80–200 km), and the smearing out from 500 to 2000 km of the high-Q zone in the intermediate mantle.

These observations, and the shape of the transformed kernels will define the directions of attack for the parameter space inversion experiments: first, it is clear

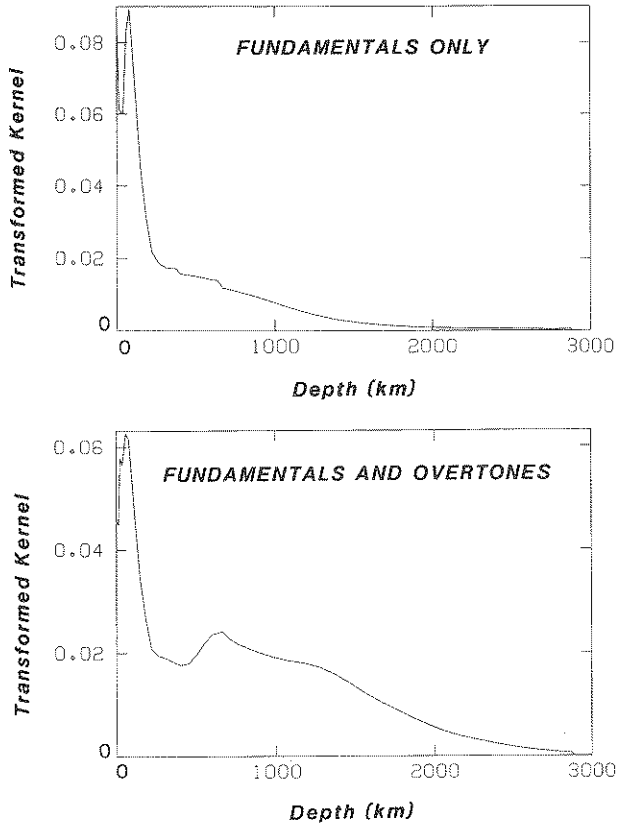

Figure 4
Transformed resolving kernels obtained in the data space inversion. *Top*: Fundamentals only. *Bottom*: Full dataset of fundamentals and overtones.

(although unfortunate) that no information can be obtained from the present dataset on the nature of the attenuation properties of the deepest parts of the mantle. Such regions as D″ will have to be investigated separately. We will not in this respect attempt to layer the mantle below 2000 km.

• *Parameter Space Inversion.* In this section, we attempt to obtain better fits to the complete dataset of fundamental and overtone Q's by letting some of the parameters of the models PREM and QKB vary, while constraining the general features of these models. We are guided in these efforts by our results from the data space inversion above.

We first attempt to refine the values of the shear attenuation Q_μ^{-1} of model PREM, without changing its layering, as given in Table 4. We use as a starting model either PREM, or QCST. We constrain Q in the crust and lid (above 80 km) to its PREM value ($Q_\mu = 600$), and solve for Q_μ in the above three layers. (The

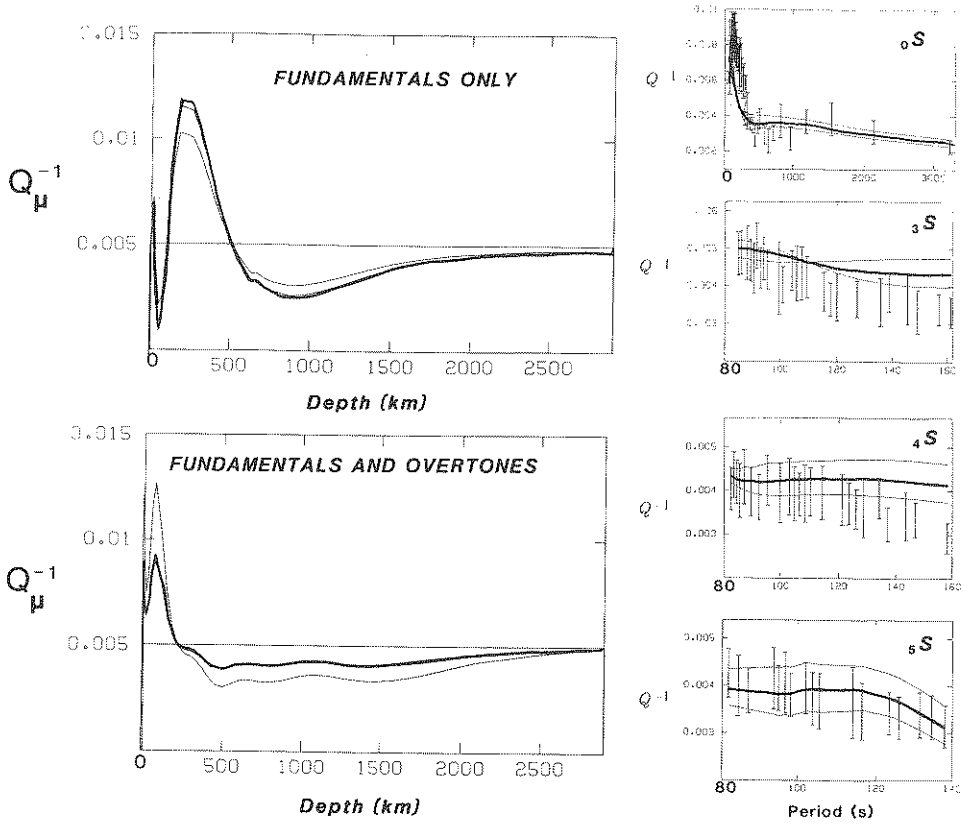

Figure 5

Results of data space inversion. *Left*: Q_μ^{-1} as a function of depth (Top: fundamentals only; Bottom: Full dataset); the horizontal line is the starting model, the thin lines the subsequent iterations, and the thick trace the final model. *Right*: Observed and computed Q^{-1} for the various branches. In all cases, the thicker line corresponds to the final solution.

reason for not solving for the crustal Q is the lack of resolution of the dataset in this area, and the expected lateral variability of this parameter; as a result, and in the case of QCST, we are actually using a two-layered starting model.) The inversion converges fast (in four iterations to 4 significant digits in the root-means-squares residual) to the model PAR1, shown on Figure 6 and Table 5, featuring a slight increase in the deeper mantle ($Q_\mu = 358$) and a 10% decrease in Q_μ in the asthenosphere ($Q_\mu = 72$). The final models derived from starting models QCST and PREM are equivalent. The inclusion of the slight amount of bulk attenuation in PREM ($Q_K = 57822$) has of course no effect on the final model. PAR1 fits the whole dataset extremely well, with the exception of the gravest fundamental modes ($_0S_l$, $l = 2$–5). Table 5 also gives the absolute value of the mean and standard deviation

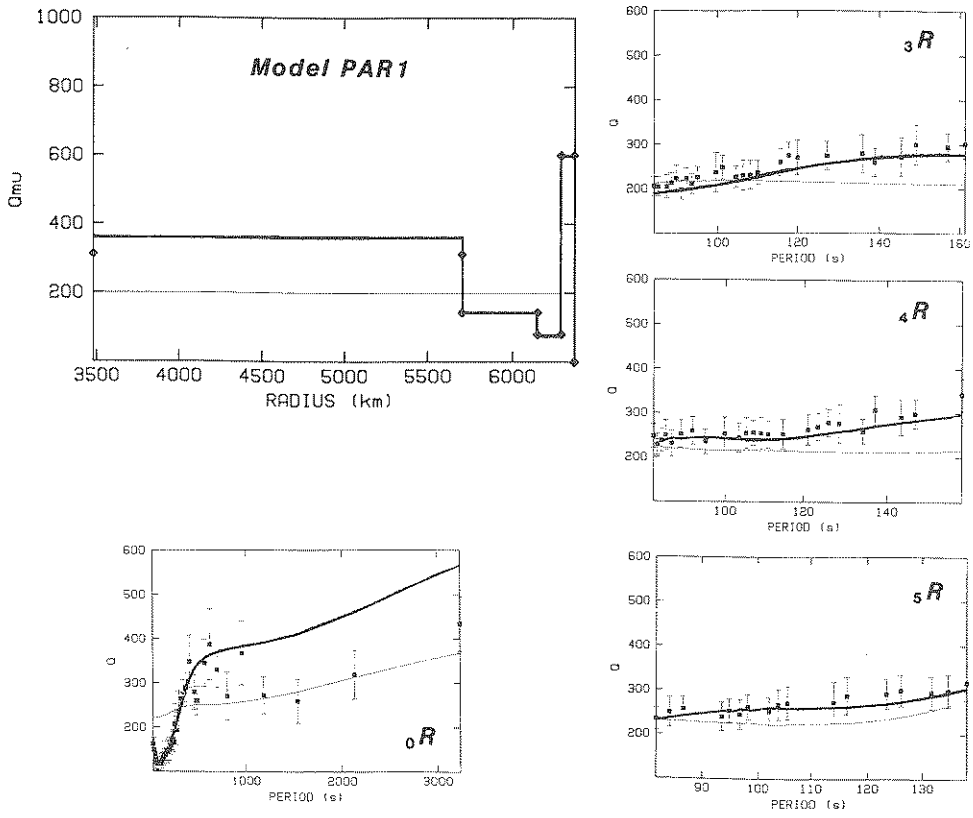

Figure 6
Results of parameter space inversion for Model PAR1. *Top Left*: Q_μ as a function of radius. The thin line corresponds to the starting model QCST. The diamonds refer to the PREM Q model. The thick line is the final model. *Bottom Left and Right*: Comparison of observed values along various branches with successive iterations. The thin line is the starting model and the thick one the final iteration.

for the relative misfits $[Q^{-1}_{\text{computed}}/Q^{-1}_{\text{observed}} - 1]$, as well as the computed value of Q_{ScS} for the various models.

Driven by our observation (see data space inversion above) of the contribution of the overtone Q's to enhanced resolution in the 1000–2000 km depth range, we then decided to increase the layering in the deeper mantle. Specifically, we now use a 6-layer solid earth, with boundaries at 500, 1000 and 2000 km depth. The resulting models obtained with QCST or PREM as starting models (PAR2C and PAR2P, respectively), are shown on Figure 7 and in Table 5. The standard deviation is significantly improved from the PAR1 model, as is the fit to the fundamentals. Note that the inversion is unable to resolve the deepest layer, and thus leaves its attenuation unaltered. This results in poorer fits for models using PREM as a starting model.

Table 5

Models inverted with QCST and PREM as starting models

Layer				
	Depth Range			
Nature	(km)	(km)	Q_μ	Q_K
PAR1 Starting Model: QCST or PREM				
Ocean	0	3	∞	57822
Crust and Lid	3	80	600	57822
LVZ	80	220	72	57822
Transition Zone	220	670	140	57822
Lower Mantle	670	2891	357	57822
Outer Core	2891	5149.5	∞	57822
Inner Core	5149.5	6371	∞	1227
Mean residual: 0.027; Standard deviation: 0.102; Q_{ScS}: 254				
PAR2C Starting Model: QCST				
Ocean	0	3	∞	57822
Crust and Lid	3	80	600	57822
LVZ	80	220	89	57822
Transition Zone	220	500	109	57822
Lower Mantle-1	500	1071	275	57822
Lower Mantle-2	1071	2071	417	57822
Lower Mantle-3	2071	2891	207	57822
Outer Core	2891	5149.5	∞	57822
Inner Core	5149.5	6371	∞	1227
Mean residual: 0.018; Standard deviation: 0.089; Q_{ScS}: 227				
PAR2P Starting Model: PREM				
Ocean	0	3	∞	57822
Crust and Lid	3	80	600	57822
LVZ	80	220	81	57822
Transition Zone	220	500	117	57822
Lower Mantle-1	500	1071	373	57822
Lower Mantle-2	1071	2071	373	57822
Lower Mantle-3	2071	2891	309	57822
Outer Core	2891	5149.5	∞	57822
Inner Core	5149.5	6371	∞	1227
Mean residual: 0.017; Standard deviation: 0.095; Q_{ScS}: 248				
PAR3C Starting Model: QCST				
Ocean	0	3	∞	57822
Crust and Lid	3	80	600	57822
LVZ	80	220	88	57822
Transition Zone	220	670	132	57822
Lower Mantle-1	670	1471	402	57822
Lower Mantle-2	1471	2071	208	57822
Lower Mantle-3	2071	2891	208	57822
Outer Core	2891	5149.5	∞	1227
Inner Core	5149.5	6371	∞	1227
Mean residual: 0.019; Standard deviation: 0.081; Q_{ScS}: 235				

Table 5 (*contd.*)

Layer (Depth Range)				
Nature	(km)	(km)	Q_μ	Q_K
PAR3P Starting Model: PREM				
Ocean	0	3	∞	57822
Crust and Lid	3	80	600	57822
LVZ	80	220	84	57822
Transition Zone	220	670	133	57822
Lower Mantle-1	670	1471	423	57822
Lower Mantle-2	1471	2071	337	57822
Lower Mantle-3	2071	2891	312	57822
Outer Core	2891	5149.5	∞	57822
Inner Core	5149.5	6371	∞	1227
Mean residual: 0.013; Standard deviation: 0.086; Q_{ScS}: 252				

The third series of models were obtained by retaining the depth 670 km as an imposed layer boundary, and moving the next boundary down to 1500 km (1471 for purposes of discretization). (The introduction of a relatively thin layer, say 670 to 1000 km would be a quest for resolution to be paid at the price of stability.) The resulting models, PAR3C, and PAR3P, are described on Figure 8 and in Table 5. Model PAR3C turned out to be our final preferred model: it achieves the best standard deviation, and provides a generally good fit to the data. Only three fundamental spheroidal modes are missed. Tests run with further layering of the mantle led to instability.

Finally, we conducted a number of experiments with SAILOR and DZIEWONSKI's (1978) model QKB as a starting model. In doing so, we incorporated finite bulk attenuation Q_K^{-1} in the inner core and the upper mantle. We did not attempt to solve for any value of Q_K, but rather to explore the effect of finite Q_K on the inverted values of Q_μ. In our first inversion, we keep QKB's layering (2 layers in the solid earth), and simply add the crust and lid layer, with a Q_μ of 600. We constrain $Q_K = 742$ in the upper mantle layer, and solve for Q_μ in the two mantle layers. This inversion is unstable: while the mean value of the residual is decreased by the iterations, the standard deviation of the residuals actually increases. This is due to the fact that the fundamentals are grossly misfit by the model.

By increasing the layering of the mantle to four layers, keeping $Q_K = 742$ in the LVZ and transition zone, and solving for the four values of Q_μ, the inversion converges on a second model, QK4L, with a relatively high standard deviation, and again failing to fit the fundamentals. This model is described in Table 6.

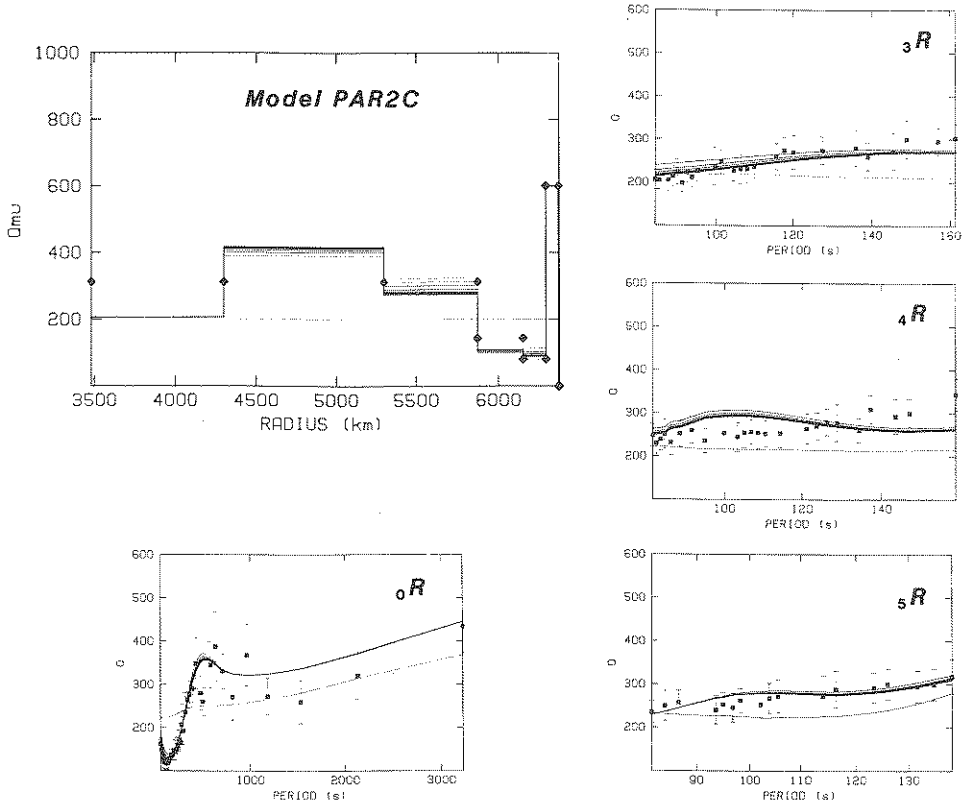

Figure 7a
Same as Figure 6, for Model PAR2C (starting model QCST). The thin lines correspond to the subsequent iterations, with the thick one referring to the final model in all diagrams.

Finally, we explored the possibility of confining the zone of finite Q_K to the seismic asthenosphere, without extending it throughout the transition zone. In the last three models studied, we use a four-layer mantle, and constrain Q_K to values of 500, 742 (used by SAILOR and DZIEWONSKI, 1978 for model QKB), and 1500 inside the LVZ (80–200 km), while solving for the four Q_μ values. Results are listed in Table 6. The resulting models (QKNR [for "narrow"], QKN2, and QKN3) give a standard residual comparable to, but not significantly better than the best PAR models. In conclusion, our dataset cannot resolve the existence of finite bulk attenuation in the mantle, and we conclude that our best model is PAR3C.

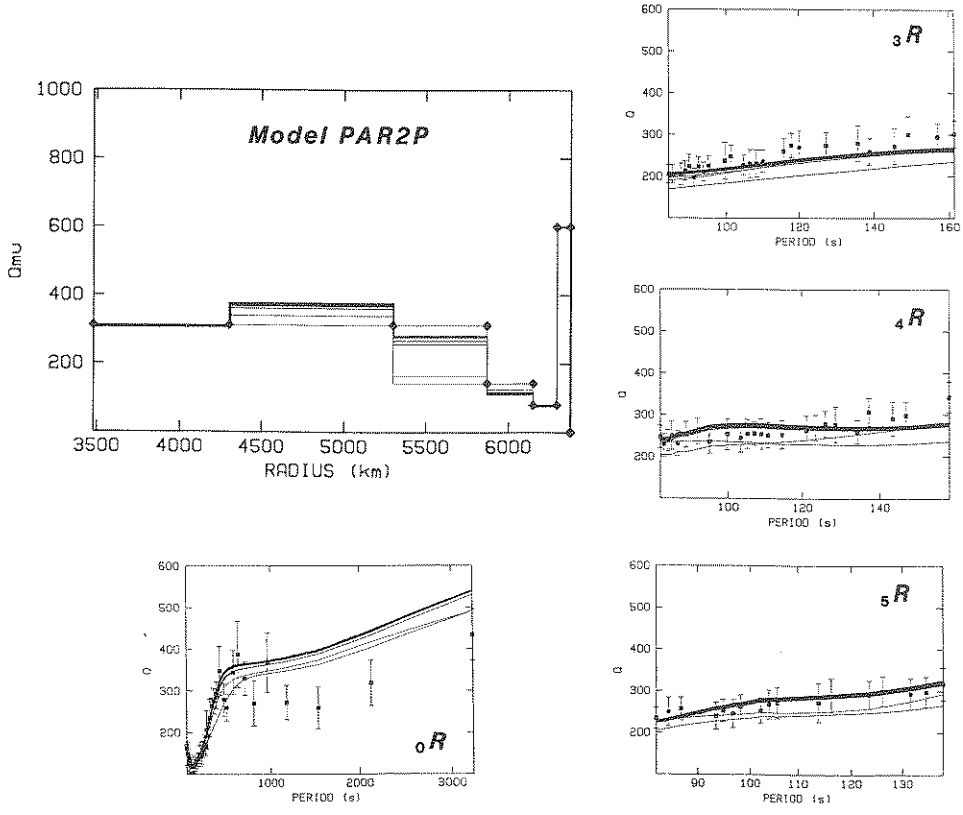

Figure 7b
Same as Figure 7a for Model PAR2P (starting model PREM).

4. Conclusions

While our dataset has limited resolution, especially in the lower mantle, its resolving kernels are sufficiently different from those obtained when using only fundamentals (e.g., STEIN *et al.*, 1981) that a number of conclusions can be drawn.

1. In general, models using QCST, rather than PREM, as starting model, provide a greater variance reduction, in the form of a lesser final value of the standard deviation. This property can be explained in the following way: while the parameter space inversion algorithm is at liberty to adapt the shear attenuation in the deepest layer of the mantle Q_{deep}^{-1}, the transformed kernels are too small in this region, and the algorithm changes Q_{deep} only insignificantly, so as not to generate instability in the pursuit of unwarranted resolution. However, models starting with different values of Q_{deep} can offer different levels of variance reduction, and their comparison can be used as an argument to resolve this

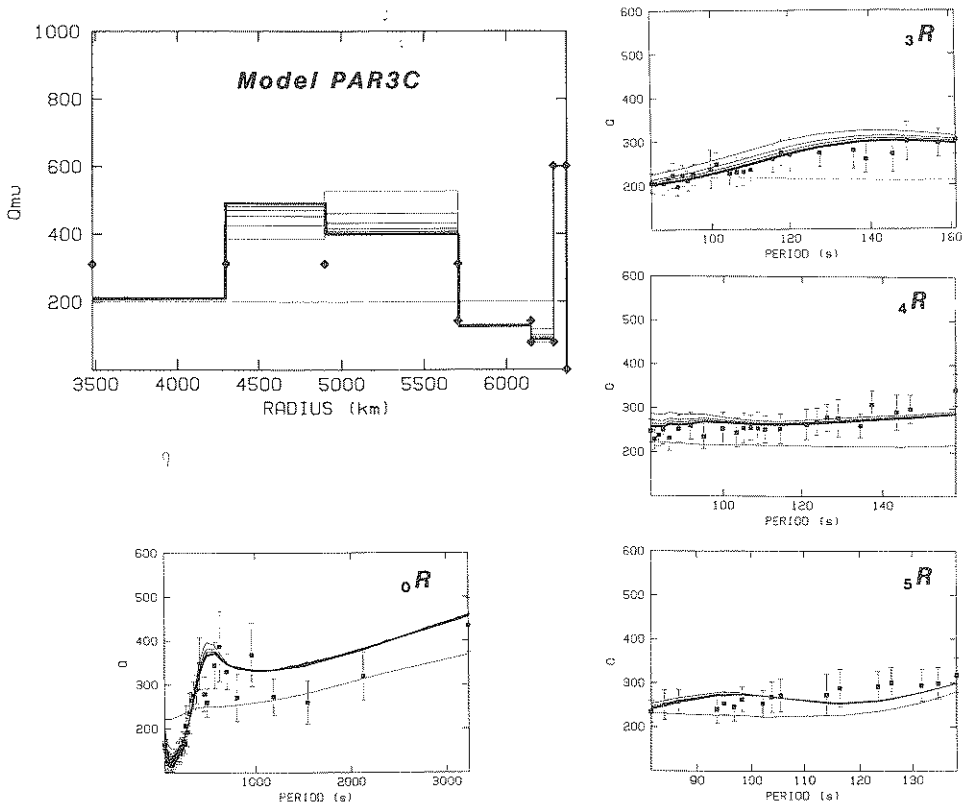

Figure 8a
Same as Figure 7a, for Model PAR3C (starting model QCST).

parameter[4]. In the present case, this suggests a Q_μ around 200, rather than 400, for the deepest mantle. The resulting values of Q_{ScS}, where the attenuation Q_μ^{-1} is integrated throughout the crust and mantle, are also in better agreement with measured values (NAKANISHI, 1979; SIPKIN and JORDAN, 1980) than for models with $Q_{\text{deep}} \sim 400$ (of course, such a comparison assumes that Q is intrinsically frequency-independent).

2. Our second conclusion regards Q_μ in the intermediate layers of the mantle (say below the transition zone). All satisfactory models feature a high Q in this

[4] There is no contradiction in saying that the formal inversion fails to constrain a parameter, and obtaining an estimate of the latter through an optimization of the residuals of a series of inversions, taken with the parameter constrained at a number of values. This procedure is indeed standard practice in retrieving hypocentral depth in earthquake location studies when the station coverage is insufficient [KANAMORI and MIYAMURA, 1970; REES and OKAL, 1987].

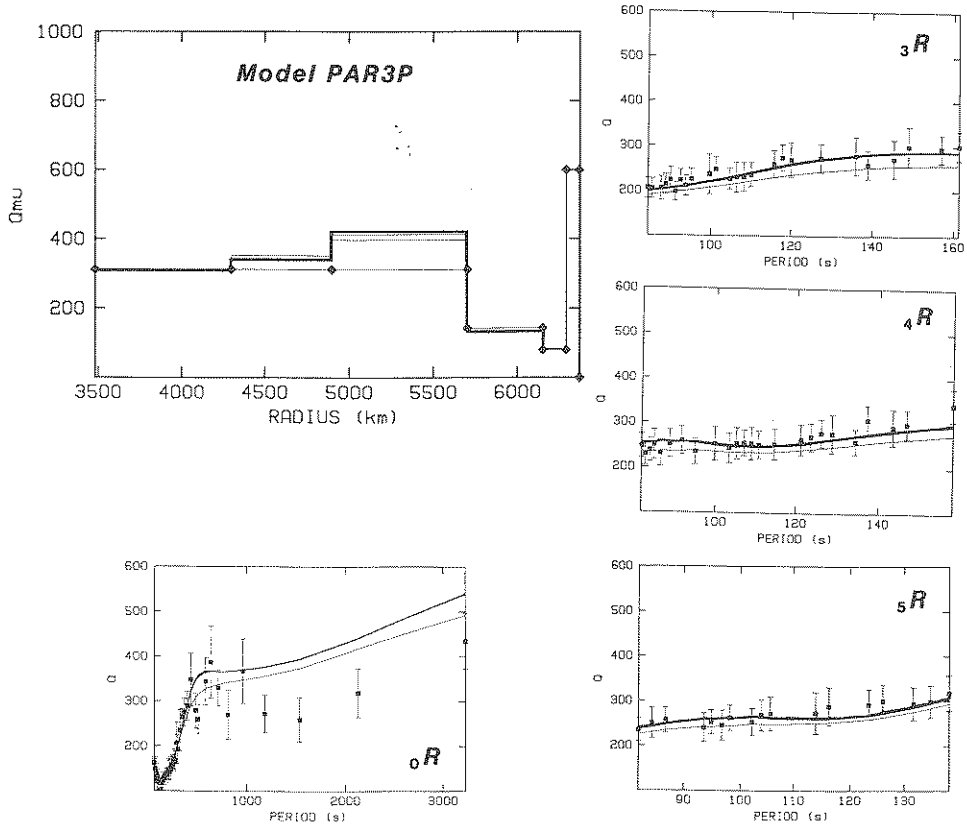

Figure 8b
Same as Figure 7a, for Model PAR3P (starting model PREM).

region, ranging from 350 to 500, regardless of which starting model is used. This figure is comparable to the minimum in attenuation obtained by STEIN *et al.* (1981), but the overtones' enhanced resolution show that it extends deeper than these authors could resolve, to at least 1500 km, and possibly 2000 km depth.

3. In addition, all models, including those starting with the flat QCST throughout the mantle, develop strong attenuation ($Q_\mu = 75-90$) in the seismic asthenosphere. This figure is fairly well constrained, and clearly makes the region the most attenuating layer of the earth. However, the models with an increased number of layers show that the transition zone has a slightly higher value of $Q_\mu = 110-140$, indicating a possible difference of temperature, thermodynamic phase, and/or composition below the "Lehman" discontinuity at 220 km.

Table 6

Models inverted with finite Q_K^{-1} and QKB as a starting model

Layer				
	Depth Range			
Nature	(km)	(km)	Q_μ	Q_K
QK2L Starting Model: QCST or PREM				
Ocean	0	3	∞	∞
Crust and Lid	3	80	600	∞
LVZ and Transition Zone	80	670	111	742
Lower Mantle	670	2891	486	∞
Outer Core	2891	5149.5	∞	∞
Inner Core	5149.5	6371	∞	1227
Mean residual: 0.048; Standard deviation: 0.125; Q_{ScS}: 257				
QK4L Starting Model: QKB				
Ocean	0	3	∞	∞
Crust and Lid	3	80	600	∞
LVZ	80	220	89	742
Transition Zone	220	670	140	742
Lower Mantle-1	670	2071	383	∞
Lower Mantle-2	2071	2891	394	∞
Outer Core	2891	5149.5	∞	∞
Inner Core	5149.5	6371	∞	1227
Mean residual: 0.031; Standard deviation: 0.092; Q_{ScS}: 271				
QKNR Starting Model: QKB				
Ocean	0	3	∞	∞
Crust and Lid	3	80	600	∞
LVZ	80	220	86	742
Transition Zone	220	670	133	∞
Lower Mantle-1	670	2071	442	∞
Lower Mantle-2	2071	2891	206	∞
Outer Core	2891	5149.5	∞	∞
Inner Core	5149.5	6371	∞	1227
Mean residual: 0.016; Standard deviation: 0.082; Q_{ScS}: 235				
QKN2 Starting Model: QKB				
Ocean	0	3	∞	∞
Crust and Lid	3	80	600	∞
LVZ	80	220	86	400
Transition Zone	220	670	135	∞
Lower Mantle-1	670	2071	449	∞
Lower Mantle-2	2071	2891	206	∞
Outer Core	2891	5149.5	∞	∞
Inner Core	5149.5	6371	∞	1227
Mean residual: 0.016; Standard deviation: 0.082; 237				

Table 6 (*contd.*)

Layer				
	Depth Range			
Nature	(km)	(km)	Q_μ	Q_K
QKN3 Starting Model: QKB				
Ocean	0	3	∞	∞
Crust and Lid	3	80	600	∞
LVZ	80	220	86	1500
Transition Zone	220	670	132	∞
Lower Mantle-1	670	2071	438	∞
Lower Mantle-2	2071	2891	206	∞
Outer Core	2891	5149.5	∞	∞
Inner Core	5149.5	6371	∞	1227
Mean residual: 0.016; Standard deviation; Q_{ScS}: 234				

4. Finally, our attempts at improving the fits by introducing bulk attenuation in the transition zone and/or low-velocity zone, are unrewarding. We must conclude that the present dataset is not a proper one for addressing this problem.

It should be noticed that in a recent study, DING and GRAND (1987), have used the amplitudes, travel times and waveforms of multiply reflected S phases to investigate Q under North America and the East Pacific. Their results, calling for Q_μ on the order of 70 in the LVZ, and more than 300 below the transition zone, are in basic agreement with ours. Since Phase X is a limit to the family of body phases which these authors use, this agreement is not surprising; it upholds *a posteriori* our methodology (including the correction for systematic bias), and confirms that intrinsic Q's are most probably frequency-independent in the period range 20–160 s separating their study from ours.

In the final conclusion, it is clear that Phase X Q values provide some improvement in the resolving power of our dataset, but these results must still be considered preliminary. The gathering of a homogeneous dataset of overtone Q's including for torsional modes, and 1st and 2nd order Rayleigh overtones, as well as for Phase X modes, will be necessary to achieve satisfactory resolution of the attenuation properties of the deep mantle.

Acknowledgments

We thank Seth Stein for discussion and for providing us with original computer codes. This study represents part of the second author's Ph.D. dissertation submitted to Yale University. This research was supported by the National Science Foundation, under Grand Number EAR–84–05040.

REFERENCES

AKI, K., and RICHARDS, P. G., *Quantitative Seismology* (San Francisco, W. H. Freeman and Co. 1980), 932 pp.

ALSOP, L. E., SUTTON, G. H., and EWING, M. (1961), *Measurement of Q for Very Long Period Free Oscillations*, J. Geophys. Res. *66*, 2911–2915.

ANDERSON, D. L., and HART, R. S. (1978), *Attenuation Models of the Earth*, Phys. Earth Planet. Inter. *16*, 289–306.

BACKUS, G., and GILBERT, J. F. (1967), *Numerical Applications of a Formalism for Geophysical Inverse Problems*, Geophys. J. Roy. Astr. Soc. *13*, 247–276.

BACKUS, G., and GILBERT, J. F. (1968), *The Resolving Power of Gross Earth Data*, Geophys. J. Roy. Astr. Soc. *16*, 169–205.

BULAND, R. P., and GILBERT, J. F. (1978), *Improved Resolution of Complex Eigenfrequencies in Analytically Continued Seismic Spectra*, Geophys., J. Roy. Astr. Soc. *52*, 457–470.

DAHLEN, F. A. (1975), *The Correction of Great-circular Surface Wave Phase Velocity Measurements for the Rotation and Ellipticity of the Earth*, J. Geophys. Res. *80*, 4895–4903.

DAHLEN, F. A. (1979), *The Spectra of Unresolved Split Normal Mode Multiplets*, Geophys. J. Roy. Astr. Soc. *58*, 1–33, 1979.

DING, X.-Y., and GRAND, S. P. (1987), *Q as a Function of Depth Beneath a Tectonically Active Area*, Eos, Trans. Am. Geophys. Un. *68*, 1376 [abstract].

DRATLER, J., FARRELL, W. E., BLOCK, B., and GILBERT, J. F. (1971), *High-Q Overtone Modes of the Earth*, Geophys. J. Roy. Astr. Soc. *23*, 399–410.

DZIEWONSKI, A. M., and ANDERSON, D. L. (1981), *Preliminary Reference Earth Model*, Phys. Earth Planet. Inter. *25*, 297–356.

DZIEWONSKI, A. M., and GILBERT, J. F. (1973), *Observations of Normal Modes from 84 Recordings of the Alaskan Earthquake of 1964 March 28.—II.: Further Remarks Based on New Spheroidal Overtone Data*, Geophys. J. Roy. Astr. Soc. *35*, 401–437.

DZIEWONSKI, A. M., FRIEDMAN, A., GIARDINI, D., and WOODHOUSE, J. H. (1983a), *Global Seismicity of 1982: Centroid-moment Tensor Solutions for 308 Earthquakes*, Phys. Earth Planet. Inter. *33*, 76–90.

DZIEWONSKI, A. M., FRANZEN, J. E., and WOODHOUSE, J. H. (1983b), *Centroid-moment Tensor Solutions for April–June, 1983*, Phys. Earth Planet. Inter. *33*, 243–249.

FUKAO, Y., and SUDA, N. (1987), *Detection of Core Modes from the Earth's Free Oscillation and Structure of the Inner Core*, Proc. XIXth Gen. Assemb. Intl. Un. Geod. Geophys., Vancouver, B.C., August 9–22, 1987. *V.I.* p. 5 [abstract].

GELLER, R. J., and STEIN, S. (1978), *Time Domain Measurements of Attenuation of Fundamental Modes* $({}_0S_6 - {}_0S_{28})$ *for the 1977 Indonesian Earthquake*, Bull. Seismol. Soc. Am. *69*, 1671–1691.

GILBERT, J. F. (1971), *Ranking and Winnowing Gross Earth Data for Inversion and Resolution*, Geophys. J. Roy. Astr. Soc. *23*, 125–128, 1971.

HANSEN, R. A., and BOLT, B. A. (1980), *Variations Between Q Values Estimated from Damped Terrestrial Eigenvibrations*, J. Geophys. Res. *85*, 5237–5243.

JO, B.-G., *Dispersion and Attenuation of Mantle Rayleigh Rayleigh Overtones*, Ph.D. Dissertation (Yale University, New Haven 1986).

JOBERT, N. (1978), *Contribution of Some Particularities in the Dispersion Curves to Numerical Seismograms Computed by Normal Modes*, J. Comput. Phys. *29*, 404–411.

JOBERT, N., and ROULT, G. (1976), *Periods and Damping of Free Oscillations Observed in France after Sixteen Earthquakes*, Geophys. J. Roy. Astr. Soc. *45*, 155–176.

JOBERT, N., GAULON, R. DIEULIN, A., and ROULT, G. (1977), *Sur des ondes à très longue période, caractéristiques du manteau supérieur*, C. R. Acad. Sci. Paris, Sér. B *285*, 49–52.

KANAMORI, H., and ANDERSON, D. L. (1977), *Importance of Physical Dispersion in Surface Wave and Free Oscillation Problems: Review*, Rev. Geophys. Space Phys. *15*, 105–112.

KANAMORI, H., and CIPAR, J. J. (1974), *Focal Process of the Great Chilean Earthquake, May 22, 1960*, Phys. Earth Planet. Inter. *9*, 128–136.

KANAMORI, H., and GIVEN, J. W. (1982), *Use of Long-period Surface Waves for Fast Determination of Earthquake Source Parameters; 2. Preliminary Determination of Source Mechanism of Large Earthquakes* ($M_s \geq 6.5$) *in 1980*, Phys. Earth Planet. Inter. *30*, 260–268.

KANAMORI, H., and MIYAMURA, S. (1970), *Seismometrical Re-evaluation of the Great Kanto Earthquake of September 1, 1923*, Bull. Earthq. Res. Inst. Tokyo Univ. *48*, 115–125.

LANCZOS, C. *Linear Differential Operators* (Van Nostrand, London 1961).

MASTERS, G., and GILBERT, J. F. (1981), *Structure of the Inner Core Inferred from Observations of its Spheroidal Shear Modes*, Geophys. Res. Letts. *8*, 569–571.

MASTERS, T. G., and GILBERT, F. (1983), *Attenuation in the Earth at Low Frequencies*, Phil. Trans. Roy. Soc. London *308A*, 479–522.

MENDIGUREN, J. A. (1973), *Identification of Free Oscillation Spectral Peaks for the 1970 July 31, Colombian Deep Shock Using the Excitation Criterion*, Geophys. J. Roy. Astr. Soc. *33*, 281–321.

MILLS, J. M., Jr., and HALES, A. L. (1977), *Great Circle Rayleigh Wave Attenuation and Group Velocity, Part I: Observations for Periods between 150 and 600 Seconds for 7 Great Circle Paths*, Phys. Earth Planet. Inter. *14*, 109–119.

MILLS, J. M., Jr., and HALES, A. L. (1978), *Great Circle Rayleigh Wave Attenuation and Group Velocity. Part II: Observations for Periods between 50 and 200 Seconds for 9 Great Circle Paths, and Global Averages for Periods of 50 to 600 Seconds*, Phys. Earth Planet. Inter. *17*, 209–231.

NAKANISHI, I. (1979), *Attenuation of Multiple ScS Beneath the Japanese Arc*, Phys. Earth Planet. Inter. *19*, 337–347.

NAKANISHI, I. (1981), *Shear Velocity and Shear Attenuation Models Inverted from the World-wide and Pure-path Average Data of Mantle Rayleigh waves* ($_0S_{25}$ *to* $_0S_{80}$) *and Fundamental Spheroidal Modes* ($_0S_2 - _0S_{24}$), Geophys. J. Roy. Astr. Soc. *66*, 83–130.

NESS, N. F., HARRISON, J. C., and SLICHTER, L. B. (1961), *Observations of the Free Oscillations of the Earth*, J. Geophys. Res. *66*, 621–629.

NOWROOZI, A. A. (1974), *Characteristic Periods and Q for Oscillations of the Earth Following an Intermediate Focus Earthquake*, J. Phys. Earth *22*, 1–23.

OKAL, E. A. (1978), *A Physical Classification of the Earth's Spheroidal Modes*, J. Phys. Earth *26*, 75–103.

OKAL, E. A. (1980), *Overtone Q's from the IDA Network*, *Eos*, Trans. Am. Geophys. Un. *61*, 1043 [abstract].

OKAL, E. A., and JO, B.-G. (1985), *Stacking Investigations of Higher-order Mantle Rayleigh Waves*, Geophys. Res. Letts. *12*, 421–424.

OKAL, E. A., and JO, B.-G. (1987), *Stacking Investigations of the Dispersion of Higher Order Mantle Rayleigh Waves and Normal Modes*, Phys. Earth Planet. Inter. *47*, 188–204.

OKAL, E. A., and STEIN, S. (1981), *Measurement and Inversion of Overtones Spheroidal Q's from IDA Records*, Eos, Trans. Am. Geophys. Un. *62*, 947 [abstract].

REES, B. A., and OKAL, E. A. (1987), *The Depth of the Deepest Historical Earthquakes*, Pure Appl. Geophys. *125*, 699–715.

ROMANOWICZ, B. A., and GUILLEMANT, P. (1984), *An Experiment in the Retrieval of Depth and Source Mechanism of Large Earthquakes Using Very Long-period Wave Data*, Bull. Seismol. Soc. Am. *74*, 417–437.

ROULT, G. (1974), *Atténuation des ondes sismiques de très basse fréquence*, Ann. Géophys. *30*, 141–167.

ROULT, G. (1975), *Attenuation of Seismic Waves of Very Low Frequency*, Phys. Earth Planet. Inter. *10*, 159–166.

SAILOR, R. V., and DZIEWONSKI, A. M. (1978), *Measurements and Interpretation of Normal Mode Attenuation*, Geophys. J. Roy. Astr. Soc. *53*, 559–581.

SILVER, P. G., and JORDAN, T. H. (1981), *Fundamental Spheroidal Mode Observations of Aspherical Heterogeneity*, Geophys, J. Roy. Astr. Soc. *64*, 605–634.

SIPKIN, S. A., and JORDAN, T. H. (1980), *Regional Variation of* Q_{ScS}, Bull. Seismol. Soc. Am. *70*, 1071–1102.

SLEEP, N. H., GELLER, R. J., and STEIN, S. (1981), *A Constraint on the Earth's Lateral Heterogeneity from the Scattering of Spheroidal Mode* Q^{-1} *Measurements* Bull. Seismol. Soc. Am. *71*, 183–197.

SMITH, S. W. (1972), *The Anelasticity of the Mantle*, Tectonophysics *13*, 601–622.

STEIN, S., and GELLER, R. J. (1978), *Attenuation Measurements of Split Normal Modes for the 1960 Chilean and 1964 Alaskan Earthquakes*, Bull. Seismol. Soc. Am. *68*, 1595–1611.

STEIN, S., and NUNN, J. A. (1981), *Analysis of Split Normal Modes for the 1977 Indonesian Earthquake*, Bull. Seismol. Soc. Am. *71*, 1031–1047.

STEIN, S., MILLS, J. M., JR., and GELLER, R. J., Q^{-1} models from data space inversion of fundamental spheroidal mode attenuation measurements, In *Anelasticity of the Earth* (eds. Stacey, F. D., Paterson, M. S., and Nicolas, A.) Geodynamics Series, *4* (Am. Geophys. Un., Washington, D.C. 1981) pp. 39–53.

TANIMOTO, T. (1987), *The Three-dimensional Shear Wave Structure in the Mantle by Overtone Waveform Inversion—I. Radical Seismogram Inversion*, Geophys. J. Roy. Astr. Soc. *89*, 713–740.

WIGGINS, R. A. (1972), *The General Linear Inverse Problem: Implications of Surface Waves and Free Oscillations for Earth Structure*, Rev. Geophys. Space Phys. *10*, 251–285.

WIGGINS, R. A. (1976), *A Fast, New Computational Algorithm for Free Oscillations and Surface Waves*, Geophys. J. Roy. Astr. Soc. *47*, 135–150.

WOODHOUSE, J. H., and DZIEWONSKI, A. M. (1984), *Mapping the Upper Mantle: Three-dimensional Modeling of Earth Structure by Inversion of Seismic Data*, J. Geophys. Res. *89*, 5953–5986.

(Received January 2, 1987, revised December 25, 1987, accepted January 14, 1988)